HYBRID RANS-LES MODELING FOR NON-EQUILIBRIUM TURBULENT FLOWS

Bruno Chaouat
Department of Computational Fluid Dynamics, ONERA
BP 72 - 92322 Châtillon cedex, France
Bruno.Chaouat@onera.fr

Roland Schiestel
IRPHE CNRS/Universités d'Aix-Marseille I & II
Technopôle Château-Gombert, BP 146 - 13384 Marseille cedex 13, France
Roland.Schiestel@irphe.univ-mrs.fr

ABSTRACT

The partially integrated transport modeling (PITM) method for subgrid turbulence quantities viewed as a continuous approach of hybrid RANS/LES methods with seamless coupling between the two extreme limits that are the full statistical and direct numerical simulation depending on the spectral cutoff location is considered (Schiestel and Dejoan, 2005). In this framework, the PITM version based on the transport equations for the turbulent stresses together with the dissipation rate equation proposed recently (Chaouat and Schiestel, 2005) is now developed in a more general formulation based on an accurate energy spectrum $E(\kappa)$ valid for both large and small eddy ranges and that allows to calibrate more accurately the $c_{sgs\epsilon_2}$ function used in the ϵ transport equation. The model is here proposed in an extended approach that can be applied to a larger range of flows by considering the turbulence length scale $L_e = k^{3/2}/(\epsilon_{sgs} + \epsilon^<)$ built by means of the total turbulent energy k and the total dissipation rate ϵ including the subgrid zone dissipation ϵ_{sgs} and the resolved part of the dissipation rate $\epsilon^<$. The present model is first tested on the decay of homogeneous isotropic turbulence referring to the experiment of Comte-Bellot and Corrsin. Then, initial perturbed spectra $E(\kappa)$ with a peak or a defect of energy are considered for analyzing the model capabilities in non-equilibrium flow situations. The second test case chosen is the well known fully turbulent channel flow that allows to assess the performance of the model in non homogeneous flows, and especially, its capacity to reproduce the flow anisotropy.

INTRODUCTION

Mathematical turbulence modeling methods such as the RANS method (Launder, 1989; Speziale, 1991) or the LES method have made significant progress in the past decade for predicting various practical turbulent shear flows. Generally, the RANS models appear well suited to handle engineering applications involving strong effects of streamline curvature, adverse pressure gradient encountered for instance in aeronautics applications (Chaouat, 2007) whereas LES subgrid models (Lesieur, 2005) are rather used for simulating academic flows with emphasis on the flow structures, the two-point correlations and the energy spectrum. All these various approaches have often been developed along independent lines and the connection between them is generally not clearly established. In this framework, the partially integrated transport modeling (PITM) for the subgrid turbulence quantities viewed as a continuous approach of hybrid RANS/LES methods with seamless coupling (Schiestel and Dejoan, 2005; Chaouat and Schiestel, 2005) gains major interest on the fundamental point of view because it bridges these different levels of description in a consistent way (Hanjalic et al., 2004; Chaouat and Schiestel, 2007) that takes advantage of RANS and LES approaches. Hybrid RANS/LES methods are now more and more widespread such as for instance the PANS model (Girimaji et al., 2006) that appeared in this line of thought with great similarities with the PITM approach. The PITM model takes its physical foundation in the spectral space that consider the Fourier transform of the two-point fluctuating velocity correlation equations with an extension to non-homogeneous turbulence (Chaouat and Schiestel, 2007). Because of its formulation, it appears well suited for simulating flows on relatively coarse grids when the spectral cutoff is located before the inertial zone.

The present paper presents the main features of the PITM that allows transposition of turbulence modeling from RANS to LES. New developments that extend the original PITM formulation (Chaouat and Schiestel, 2005) to a larger range of flows are then proposed.

PITM APPROACH TO SUBGRID-SCALE TURBULENCE MODELS

General formalism

For large eddy simulations, the spectrum is partitioned using a cutoff wave number κ_c. In classical LES, this cutoff is located in the beginning of the inertial range of eddies but in the present approach, like in very large eddy simulations (VLES), the cutoff may be located before the inertial range. Another wave number κ_d located at the end of the inertial range of the spectrum is also used, assuming that the energy pertaining to higher wavenumbers is entirely negligible. This practice, inspired from multiple scale modeling (Schiestel, 1987) avoids considering infinite limits and molecular viscosity effects in the far end of the spectrum. When non-homogeneous turbulence is considered (this is indeed the usual case), the concept of tangent homogeneous space at a point of the non-homogeneous flow field is used (Chaouat and Schiestel, 2007). One may remark also that the cutoff is not necessarily equal to the grid spacing, it can be dissociated in a subfilter model. In this case, it is then possible to define the large scale fluctuations (resolved scales) $u_i^<$ and the fine scales (modeled scales) $u_i^>$ through the relations using the wave number $\boldsymbol{\kappa}$

$$u_i^< = \int_{|\kappa|\leq\kappa_c} \widehat{u'}_i(\boldsymbol{X},\boldsymbol{\kappa}) \exp\left(j\boldsymbol{\kappa\xi}\right) d\boldsymbol{\kappa} \tag{1}$$

$$u_i^> = \int_{|\kappa|\geq\kappa_c} \widehat{u'}_i(\boldsymbol{X},\boldsymbol{\kappa}) \exp\left(j\boldsymbol{\kappa\xi}\right) d\boldsymbol{\kappa} \tag{2}$$

When the cutoff vanishes, the full integration in the tangent homogeneous space exactly corresponds to the statistical mean, that guarantees exact compatibility with RANS equations. In this framework, the instantaneous velocity u_i is decomposed into a statistical part $\langle u_i \rangle$, a large scale fluctuating $u_i^<$ and a small scale fluctuating $u_i^>$ such that $u_i = \langle u_i \rangle + u_i^< + u_i^>$. The first two terms correspond to the filtered velocity $\bar{u}_i$ such that $\bar{u}_i = \langle u_i \rangle + u_i^<$. The velocity fluctuation u_i' contains a large-scale and a small-scale parts, $u_i' = u_i^< + u_i^>$. This particular filter, as a spectral truncation, presents some additional useful properties that are not verified for progressive filters. In particular, the large scale and small scale fluctuations are uncorrelated (Schiestel, 1987) $\langle \varphi^> \psi^< \rangle = 0$ implying for instance the relation

$$R_{ij} = \langle u_i u_j \rangle - \langle u_i \rangle \langle u_j \rangle = \langle u_i' u_i' \rangle = \left\langle u_i^< u_j^< \right\rangle + \left\langle u_i^> u_j^> \right\rangle \tag{3}$$

The transport equation for the filtered Navier-Stokes equations takes the form

$$\frac{\partial \bar{u}_i}{\partial t} + \frac{\partial}{\partial x_j}\left(\bar{u}_i\bar{u}_j\right) = -\frac{1}{\rho}\frac{\partial \bar{p}}{\partial x_i} + \nu\frac{\partial^2 \bar{u}_i}{\partial x_j \partial x_j} - \frac{\partial \tau_(u_i,u_j)}{\partial x_j} \tag{4}$$

in which, following Germano's derivation (Germano, 1992), the subgrid-scale tensor is defined by the relation

$$(\tau_{ij})_{sgs} = \tau(u_i,u_j) = \overline{u_i u_j} - \bar{u}_i\bar{u}_j \tag{5}$$

As a result of interest, the transport equation for the subgrid-scale tensor takes a generic form if written in terms of central moments (Germano, 1992). So that, the resulting equation can be rearranged as

$$\begin{aligned}
\frac{\partial \tau(u_i,u_j)}{\partial t} + \frac{\partial}{\partial x_k}\left[\tau(u_i,u_j)\bar{u}_k\right] = \\
-\tau(u_i,u_k)\frac{\partial \bar{u}_j}{\partial x_k} - \tau(u_j,u_k)\frac{\partial \bar{u}_i}{\partial x_k} \\
+\tau\left(p, \frac{\partial u_i}{\partial x_j} + \frac{\partial u_j}{\partial x_i}\right) \\
-\frac{1}{\rho}\frac{\partial \tau(p,u_i)}{\partial x_j} - \frac{1}{\rho}\frac{\partial \tau(p,u_j)}{\partial x_i} - \frac{\partial \tau(u_i,u_j,u_k)}{\partial x_k} \\
+\nu\frac{\partial^2 \tau(u_i,u_j)}{\partial x_k \partial x_k} - 2\nu\tau\left(\frac{\partial u_i}{\partial x_k}, \frac{\partial u_j}{\partial x_k}\right)
\end{aligned} \tag{6}$$

with the general definition $\tau(f,g) = \overline{fg} - \bar{f}\bar{g}$ and $\tau(f,g,h) = \overline{fgh} - \bar{f}\tau(g,h) - \bar{g}\tau(h,f) - \bar{h}\tau(f,g) - \bar{f}\bar{g}\bar{h}$ for any turbulent quantities f, g, h. Equation (6) will then be solved numerically in space and time. Using the definition $D/Dt = \partial/\partial t + \bar{u}_k \partial/\partial x_k$, equation (6) reads

$$\frac{D(\tau_{ij})_{sgs}}{Dt} = (P_{ij})_{sgs} + (\Psi_{ij})_{sgs} + (J_{ij})_{sgs} - (\epsilon_{ij})_{sgs} \tag{7}$$

where in this equation, the production term $(P_{ij})_{sgs}$ is given by

$$(P_{ij})_{sgs} = -(\tau_{ik})_{sgs}\frac{\partial \bar{u}_j}{\partial x_k} - (\tau_{jk})_{sgs}\frac{\partial \bar{u}_i}{\partial x_k} \tag{8}$$

The corresponding equation for the subfilter energy is obtained by half the trace

$$\frac{Dk_{sgs}}{Dt} = P_{sgs} + J_{sgs} - \epsilon_{sgs} \tag{9}$$

where $P_{sgs} = (P_{mm})_{sgs}/2$ and $\epsilon_{sgs} = (\epsilon_{mm})_{sgs}/2$. Because of the nice properties of the truncation filter in Fourier space, one can see that the mean statistical and filtered equations can both be written in a similar form. As a consequence, the closure approximations used for the statistical partially averaged equations are assumed to prevail also in the case of large eddy numerical simulations. The present formalism is indeed the essence of the PITM model, first developed by Schiestel and Dejoan (2005) for the transport equation (9) of the subgrid-scale turbulent energy k_{sgs} and subsequently by Chaouat and Schiestel for the transport equation (7) of the subgrid-scale turbulent stress tensor $(\tau_{ij})_{sgs}$.

Stress transport equation subfilter model

In the subfilter models, as usual in statistical approaches, the redistribution term $(\Psi_{ij})_{sgs}$ which appears in equation (7) is decomposed into a slow part $(\Psi_{ij}^1)_{sgs}$ and a rapid part $(\Psi_{ij}^2)_{sgs}$ in the subgrid-scale range. This term is modeled in the range $[\kappa_c, \kappa_d]$ where the wave number κ_d is located at the end of the inertial range of the spectrum after the transfer zone. The cutoff wave number is generally computed from the grid size such as $\kappa_c = \pi/\Delta$ where $\Delta = (\Delta_1\Delta_2\Delta_3)^{1/3}$. The slow term is modeled assuming that usual statistical Reynolds stress models must be recovered in the limit of vanishing cutoff wave number κ_c and also that the return to isotropy is increased at higher wave numbers, as also assumed in multiple-scale models (Schiestel, 1987)

$$(\Psi_{ij}^1)_{sgs} = -c_{sgs_1}\frac{\epsilon_{sgs}}{k_{sgs}}\left((\tau_{ij})_{sgs} - \frac{1}{3}(\tau_{mm})_{sgs}\delta_{ij}\right) \tag{10}$$

$$(\Psi_{ij}^2)_{sgs} = -c_2\left((P_{ij})_{sgs} - \frac{1}{3}(P_{mm})_{sgs}\delta_{ij}\right) \tag{11}$$

where c_{sgs_1} is now a continuous function of the dimensionless parameter $\eta_c = \kappa_c L_e$ involving the turbulence length scale $L_e = k^{3/2}/(\epsilon_{sgs} + \epsilon^<)$ built by means of the total turbulent energy $k = k_{sgs} + k_{les}$ and the total dissipation rate ϵ including the dissipation in the subgrid zone ϵ_{sgs}, and the resolved part of the dissipation rate $\epsilon^< = \nu(\partial u_i^< \partial u_i^< / \partial x_j \partial x_j)$ for the large-scale fluctuating velocities $u_i^<$ that may be not negligible in low Reynolds number flows. According to the classical physics of turbulence, the coefficient c_{sgs_1} must increase with the parameter η_c in order to increase the return to isotropy in the range of larger wave numbers. To do that, we suggest a simple empirical function

$$c_{sgs_1} = \frac{1 + \alpha_\eta\,\eta_c^2}{1 + \eta_c^2}c_1 \tag{12}$$

where α_η is a numerical constant. This function satisfies the limiting condition $\lim_{\eta_c \to 0} c_{sgs_1}(\eta_c) = c_1$. As usual, the diffusion process $(J_{ij})_{sgs}$ is modeled assuming a gradient law

$$(J_{ij})_{sgs} = \frac{\partial}{\partial x_k}\left(\nu\frac{\partial(\tau_{ij})_{sgs}}{\partial x_k} + c_s\frac{k_{sgs}}{\epsilon_{sgs}}(\tau_{kl})_{sgs}\frac{\partial(\tau_{ij})_{sgs}}{\partial x_l}\right) \tag{13}$$

where c_s is a numerical coefficient which takes the value 0.22. Moreover, we assume $(\epsilon_{ij})_{sgs} = (2/3)\epsilon_{sgs}\delta_{ij}$. In contrast with the two-equation model, it can be mentioned that the production term $(P_{ij})_{sgs}$ is allowed to become negative. In such a case, this implies that energy is transferred from the filtered motions up to the resolved motions, known as backscatter process. Closure of equation (7) is necessary for the dissipation-rate which is computed by means of a transport equation. The dissipation-rate ϵ_{sgs} is therefore used for calculating the length scale without referring directly to the mesh size. That allows to simulate non-equilibrium flows when the filter width is no longer a good estimate of the characteristic turbulence length. As a result of the modeling (Chaouat and Schiestel, 2005), the modeled transport equation for the dissipation-rate ϵ_{sgs} taking into account the convective and diffusive processes reads

$$\frac{D\epsilon_{sgs}}{Dt} = c_{\epsilon_1}\frac{\epsilon_{sgs}}{k_{sgs}}\frac{(P_{mm})_{sgs}}{2} - c_{sgs\epsilon_2}\frac{\epsilon_{sgs}^2}{k_{sgs}} + (J_\epsilon)_{sgs} \quad (14)$$

where

$$(J_\epsilon)_{sgs} = \frac{\partial}{\partial x_j}\left(\nu\frac{\partial \epsilon_{sgs}}{\partial x_j} + c_\epsilon \frac{k_{sgs}}{\epsilon_{sgs}}(\tau_{jm})_{sgs}\frac{\partial \epsilon_{sgs}}{\partial x_m}\right) \quad (15)$$

In equation (14), $c_{sgs\epsilon_2}$ is now a function of the dimensionless cutoff wave number η_c. Intuitively, it is obvious that the usual ϵ equation used in statistical modeling in which the whole spectrum is modeled cannot be used without modification in LES in which just a part of the spectrum is modeled. This modification is made through a variation of the coefficient $c_{sgs\epsilon_2}$ and so the model is then able to "read "the size of the mesh in order to model only the appropriate portion of the turbulence field. This is the main feature of PITM approaches which are basically different from an URANS approach. The mathematical physics formalism developed in the spectral space for the two-point tensor correlation $\phi_{ij} = \left\langle \widehat{u'}_i(\boldsymbol{X},\boldsymbol{\kappa})\widehat{u'}_j(\boldsymbol{X},\boldsymbol{\kappa})\right\rangle$, where $\widehat{u'}_i$ denotes the Fourier transform of the fluctuating velocity u'_i, shows (Chaouat and Schiestel, 2007) that the approach can be developed consistently in non-homogeneous turbulence.

Improved spectral model

The analytical development of the dissipation rate equation (Schiestel and Dejoan, 2005) shows that the coefficient $c_{sgs\epsilon_2}$ takes the expression

$$c_{sgs\epsilon_2} = c_{\epsilon_1} + \frac{k_{sgs}}{k}\left(c_{\epsilon_2} - c_{\epsilon_1}\right) \quad (16)$$

In the present PITM formulation, the form of the function k_{sgs}/k in equation (16) has been improved and is now evaluated by means of an accurate energy spectrum $E(\kappa)$ inspired from Von Karman like spectrum valid on the entire range of wavenumbers

$$E(\kappa) = \frac{\frac{2}{3}\beta_\eta L_e^3\, k\, \kappa^2}{\left[1+\beta_\eta(\kappa\, L_e)^3\right]^{11/9}} \quad (17)$$

where β_η is a constant coefficient, instead of simply referring to the Kolmogorov law valid in the inertial range $E(\kappa) = C_K\epsilon^{2/3}\kappa^{-5/3}$ as made previously (Chaouat and Schiestel, 2005). The subgrid-scale turbulent kinetic energy is then computed by integrating the spectrum $E(\kappa)$ in the wave number range $[\kappa_c, +\infty[$, $k_{sgs} = \int_{\kappa_c}^{\infty} E(\kappa)d\kappa = 1/\left[1+\beta_\eta(\kappa_c\, L_e)^3\right]^{2/9}$, providing the new expression of $c_{sgs\epsilon_2}$, as a function of the dimensionless cutoff wave number η_c

$$c_{sgs\epsilon_2}(\eta_c) = c_{\epsilon_1} + \frac{c_{\epsilon_2} - c_{\epsilon_1}}{\left[1+\beta_\eta\, \eta_c^3\right]^{2/9}} \quad (18)$$

where $c_{\epsilon_1} = 1.4$ and $c_{\epsilon_2} = 1.9$. In order to satisfy the correct asymptotic behavior for the spectrum $E(\kappa)$, $\lim_{\kappa\to\infty} E(\kappa) = C_K\epsilon^{2/3}\kappa^{-5/3}$, the coefficient β_η is found to take the theoretical value $\beta_\eta = (2/3C_K)^{9/2} \approx 0.026$. So that, the stress transport equation subfilter model is finally based on the modeled equations (7) and (14). Figure 1 describes the evolution of the analytical dimensionless spectrum $E(\kappa)/(kL_e)$ defined by the relation (17) as well as the Kolmogorov slope in $C_k\epsilon^{2/3}\kappa^{-5/3}$, versus the dimensionless wave number $\kappa\, L_e$. As expected, it appears that the analytical spectrum slope goes to the Kolmogorov slope for high wave numbers showing that the inertial zone is rapidly reached. In practice, several trial and error tests have been made for selecting appropriate values for the two model coefficients α_η and β_η. These tests have lead to the optimized coefficient values $\alpha_\eta = 1.5$ and $\beta_\eta = (2/3C_k)^{9/2} = 0.161$ for $C_k = 1$.

Limiting behavior

Keeping the tangent homogeneous space in mind, one can remark finally that for the case of LES performed on very large filter widths, the filter width need to be dissociated from the grid itself, because the grid must always be fine enough to capture the mean flow non-homogeneities. When the cutoff location is large then, limiting behaviors are obtained. The length scale $k_{sgs}^{3/2}/\epsilon_{sgs}$ is equal to

$$\frac{k_{sgs}^{3/2}}{\epsilon_{sgs}} = \frac{k^{3/2}}{\epsilon_{sgs}}\left(\frac{k_{sgs}}{k}\right)^{3/2} \quad (19)$$

Taking into account the limiting value $k_{sgs}/k \approx 3/2C_k\eta_c^{-2/3}$ when $k_{sgs} \ll k$, equation (19) shows that the subgrid characteristic length scale goes to the filter width

$$k_{sgs}^{3/2}/\epsilon_{sgs} = (3C_K/2)^{3/2}\,\Delta/\pi \quad (20)$$

Moreover, the definition of subfilter viscosity implies $\nu_{sgs}^{3/2} = c_\nu^{3/2}(k_{sgs}^3/\epsilon_{sgs}^{3/2}) = c_\nu^{3/2}\left(k_{sgs}^3/\epsilon_{sgs}^2\right)\epsilon_{sgs}^{1/2}$ or $\nu_{sgs} = c_\nu^{3/2}\left(k_{sgs}^3/\epsilon_{sgs}^2\right)(\epsilon_{sgs}/\nu_{sgs})^{1/2}$. Using then the previous result on the length-scale together with the hypothesis of equilibrium $\epsilon_{sgs} = 2\nu_{sgs}\left\langle \bar{S}_{i,j}\bar{S}_{i,j}\right\rangle$ where $\bar{S}_{ij} = (\partial\bar{u}_i/\partial x_j + \partial\bar{u}_j/\partial x_i)/2$, one finds that the limiting behavior for the subgrid viscosity ν_{sgs} is simply the Smagorinsky model

$$\nu_{sgs} = \frac{1}{\pi^2}\left(\frac{3C_K}{2}\right)^3 c_\nu^{3/2}\Delta^2\left[2\left\langle \bar{S}_{ij}\bar{S}_{ij}\right\rangle\right]^{1/2} \quad (21)$$

NUMERICAL METHOD

The finite volume technique is adopted for solving the full transport equations in a conservative formulation. The governing equation are integrated explicitly in time using a fourth-order Runge-Kutta scheme which is well appropriate for simulating unsteady flows. The numerical scheme is based on a centered formulation with second-order accuracy in space discretization that allows to minimize the dissipative and dispersive numerical errors. Note that an upwind scheme with second order space discretization is however retained for solving the turbulent equations (7) and (14). Because of the filtered velocity gradients $\partial\bar{u}_i/\partial x_j$ that evolves rapidly in time, the turbulent equations are difficult to solve. In that case, it is more efficient, from a numerical point of view, to solve first the redundant equation (9) and equation (14) that are strongly coupled and afterwards to solve equation (7) using the preceding k_{sgs}^* and ϵ_{sgs}^* values. In particular the Rotta term in the stress equations will be proportional to $\left((\tau_{ij})_{sgs} - \frac{2}{3}k_{sgs}^*\delta_{ij}\right)$. Still with the aim to improve the numerical scheme stability, it is also useful to average in time the ratio $T = k_{sgs}/\epsilon_{sgs}$ that appears in equation (14). This numerical procedure is of practical interest when performing LES using the PITM model. Note that this procedure can also be justified from a physical point of view since the ratio $T = k_{sgs}/\epsilon_{sgs}$ can be view as a characteristic time-scale of the turbulence. The source terms in equation (7) are linearized to avoid numerical instabilities. Equation (7), rewritten in the compact form

$$\frac{\partial(\tau_{ij})_{sgs}}{\partial t} = A - Q\ (\tau_{ij})_{sgs} \qquad (22)$$

where A and Q denotes two matrix functions of the quantities $(\tau_{ij})_{sgs}$, k^*_{sgs} and ϵ^*_{sgs} is solved using the Jacobi iterative implicit method. Indeed, by using the matrix decomposition $Q = D + R$ where D denotes a diagonal matrix and R a non-diagonal matrix, $(\tau_{ij})^{p+1}_{sgs}$ is then solution of the iterative equation

$$(\tau_{ij})^{p+1}_{sgs}[I + D\,\delta t] = (\tau_{ij})^{n}_{sgs} + [A\ -\ R\,(\tau_{ij})^{p}_{sgs}]\delta t \qquad (23)$$

where I is the identity matrix. The convergence is then assumed when $(\tau_{ij})^{n+1}_{sgs} = \lim_{p\to\infty}(\tau_{ij})^{p}_{sgs}$. Obviously, the numerical procedure much also satisfy the trace equality $k^{n+1}_{sgs} = (\tau_{nn})^{n+1}_{sgs}/2$ practically obtained within two or three internal iterations.

SIMULATION OF HOMOGENEOUS TURBULENCE

Decay of isotropic non-perturbed spectrum

The present PITM model is first tested in its two-equation contracted form defined by equations (9) and (14) in the case of decay of homogeneous isotropic turbulence referring to the experiment of Comte-Bellot (Comte-Bellot and Corrsin, 1971) to check the behavior of the model (not concerned with the anisotropy aspects). Three-dimensional turbulent energy spectra have been measured at different time advancement and the initial Reynolds number $R_t = k^2/(\nu\epsilon)$ is about 792. The PITM simulation is performed on a medium grid $N = 80^3$ for a box-size $L = 1.256$ m. The wave-numbers are defined by $\kappa = 2\pi/n$ where n varies from $-N/2+1$ to $N/2$ leading to a minimum wave-number $\kappa_{min} = 2\pi/(N\Delta) = 0.05$ cm^{-1} and a maximum wave-number $\kappa_{max} = \pi/\Delta = 2$ cm^{-1} of the grid. In the present case, a large cutoff wave-number is retained, $\kappa_c = \kappa_{max} = 2$ cm^{-1}, so that the initial ratio to the subgrid-scale energy to the total energy k_{sgs}/k is about 0.36. The initial velocity field has been produced from a random generator enforcing the given energy spectrum. Figure 2 shows the evolution of the computed three-dimensional spectra from the initial time (tU_0/M =42) for the two time advancements (tU_0/M =98, 171) compared to the Comte-Bellot data. One can observe that the numerical spectrum computed at the time tU_0/M =98 agrees well with the data in the Comte-Bellot experiment but the other one computed at the time advancement tU_0/M =171 slightly deviates from the data. In fact, a more deeply investigation reveals that the numerical slope computed at tU_0/M =171 exactly corresponds to the $\kappa^{-5/3}$ Kolmogorov slope, as it can be seen on this figure. There is no definite physical explanation unless perhaps to remark that the Comte-Bellot experiment is worked out at a relatively low Reynolds number. For this case, this implies that the inertial zone transfer is very short. Figure 3 shows the time decay of the turbulence, respectively for the subgrid-scale energy k_{sgs}, the resolved-scale energy k_{les} and the total energy in logarithmic coordinates. The decay law given by the standard $k-\epsilon$ model according to the relation $k/k_0 = t^{1/(1-c_{\epsilon_2})}$ (where k is obtained in the present LES by the sum of the subgrid and resolved-scales) leads to the slope of decay close to n=1.1 that corresponds to the usual value $\epsilon_2 = 1.90$.

Decay of isotropic perturbed spectrum

In this case, the initial Comte-bellot spectrum (α) at $tU_0/M = 42$ is artificially perturbed by modifying the energy levels departing from usual equilibrium spectrum. The aim is to study the influence of initial spectral distribution on the decay law as an illustration of out of spectral equilibrium situations. Relative to the non-perturbed spectrum (α), the initial spectra are therefore modified, respectively, by increasing the large-scales (β) or by decreasing the large scales (γ). The PITM results as well as the initial perturbed spectrum are plotted in figure 4. A first observation reveals that the different curves associated to the two perturbed spectra (β) and (γ) are both identical at the beginning of decay but afterwards are departing from the decay curve corresponding to the non-perturbed spectrum (α). As a result of interest, one can observe that a peak in large scale energy (resp. a defect in large scale energy) implies a decrease (resp. an increase) of the decay rate of turbulence. These results are found to be in qualitative agreement with EDQNM spectral models predictions (Cambon et al., 1981). These evolutions can be easily explained if one consider that the differentiation between the curves can only occur after the decay time that is required to reach the perturbed energy zone (source or sink) of the three-dimensional spectrum. Then, the curves deviate from each other because the small-scale energy decreases more rapidly than the large scale energy as indeed the time scale of small eddies is shorter. As known, note that this turbulence spectral effect due to departure from equilibrium cannot be reproduced using standard single-scale statistical turbulence models.

SIMULATION OF NON-HOMOGENEOUS TURBULENCE

Low Reynolds PITM model

In this section, the present Reynolds stress PITM model based on the transport equations (7) and (14) is applied for performing numerical simulations of the fully developed turbulent channel flow. However, these equations must be modified to account for wall effects at low turbulent Reynolds number. To do that, like in the Launder and Shima model (Launder and Shima, 1989), the function c_1 in equation (12) depends on the second and third subgrid-scale invariants $A_2 = a_{ij}a_{ji}$, $A_3 = a_{ij}a_{jk}a_{ki}$ and the flatness parameter $A = 1 - \frac{9}{8}(A_2 - A_3)$ where $a_{ij} = ((\tau_{ij})_{sgs} - \frac{2}{3}k_{sgs}\delta_{ij})/k_{sgs}$. Moreover, the term $(\Psi_{ij})^{w}_{sgs}$ that takes into account the wall reflection effect of the pressure fluctuations is embedded in the model for reproducing correctly the logarithmic region of the turbulent boundary layer.

Fully turbulent channel flow

The numerical simulation is performed on a medium mesh resolution requiring $32 \times 64 \times 84$ grids with different spacings Δ_i. The uniform dimensionless spacings in the streamwise and spanwise directions are $\Delta_1^+ = 50.9$, $\Delta_2^+ = 25.1$. In the normal direction to the wall, the grid points are distributed in nonuniform spacing with refinement near the walls. The first point is located at the dimensionless distance $\Delta_3^+ = 0.5$. The PITM simulation is compared with the DNS data (Moser et al, 1999) for a Reynolds number $R_\tau = 395$. Figure 5 displays the evolution of the subgrid-scale coefficient $c_{sgs\epsilon_2}$ obtained from relation (16) and indicates that the PITM model (with this particular choice of grid) behaves like quasi-RSM model near the walls and LES near the center of the channel since the coefficient $c_{sgs\epsilon_2}$ decreases from its RANS value to c_{ϵ_1}. The mesh size $\Delta = \pi/\kappa_c$ and the subgrid length scale $L_{sgs} = \pi(3C_k/2)^{-3/2}k_{sgs}^{3/2}/\epsilon_{sgs}$ computed from equation (20) are plotted in figure 6 versus the channel height. As a result, one can see that these two scales present different evolutions confirming the interest to compute the length-scale from the dissipation-rate equation (14) although the length scales are of the same order of magnitude. Figure 7 reveals the sharing out of turbulent energy among the subgrid and resolved turbulence scales. Note that the anisotropy of the subgrid-stresses is well reproduced because the PITM discards the concept of eddy viscosity. Figure 8 describes the evolution of the total turbulent stresses τ_{11}, τ_{22} and τ_{33} in the channel with DNS comparisons at Reynolds number $R_\tau = 395$. As shown, a very good agreement is obtained with the DNS data confirming that the total energy is well estimated.

CONCLUSION

The PITM approach viewed as a continuous hybrid RANS/LES model has been developed in a more general formulation based on an accurate energy spectrum $E(\kappa)$ and a turbulence length scale $L_e = k^{3/2}/(\epsilon_{sgs} + \epsilon^<)$ that is computed at each time advancement. This model has been calibrated and successfully tested on decay of homogeneous isotropic turbulence referring to the Comte-Bellot experiment and applied in situation of non-equilibrium flow. The performance of the model and especially, its capabilities in the anisotropy prediction have been demonstrated in the fully turbulent channel flow test case. So that, it looks as a good candidate for simulating turbulent flows that presents complex physics, providing the numerical scheme is sufficiently stable and accurate.

REFERENCES

Cambon C., Jeandel, D. and Mathieu, J., 1981, "Spectral Modelling of Homogeneous Non-Isotropic Turbulence.", *Journal of Fluid Mechanics*, Vol. 104, pp. 247-262.

Chaouat, B., and Schiestel, R., 2005, "A New Partially Integrated Transport Model for Subgrid-Scale Stresses and Dissipation Rate for Turbulent Developing Flows", *Physics of Fluids*, Vol. 17, n°6, 065106.

Chaouat, B., 2007, "Reynolds Stress Transport Modeling for High-Lift Airfoil Flows", *AIAA Journal*, Vol. 44, n°10, pp. 2390-2403.

Chaouat, B., and Schiestel, R., 2007, "From Single-Scale Turbulence Models to Multiple-Scale and Subgrid-Scale Models by Fourier Transform", *Theoretical and Computational Fluid Dynamics*, Vol. 21, n°3, pp. 201-229.

Comte-Bellot, G. and Corrsin, S., 1971, "Simple Eulerian Time Correlation of Full and Narrow-Band Velocity Signals in Grid-Generated, Isotropic Turbulence", *Journal of Fluid Mechanics*, Vol. 48, pp. 273-337.

Germano, M., 1992, "Turbulence: the Filtering Approach", *Journal of Fluid Mechanics*, Vol.238, pp. 325-336.

Girimaji, S. S., Jeong, E. and Srinivasan R., 2006 "Partially Averaged Navier-Stokes Method for Turbulence: Fixed Point Analysis and Comparison with Unsteady Partially Averaged Navier-Stokes.", *ASME*, Vol. 73, n°3, pp. 422-429.

Hanjalic, K., Hadziabdic, M., Temmerman, M. and Leschziner, M., 2004, "Merging LES and RANS Strategies: Zonal or Seamless Coupling ?", *Direct and Large eddy Simulations n° V*, Ed. by R. Friedrich, B. Geurts and O. Métais, Kluwer Academic.

Launder, B. E., 1989, "Second Moment Closure: Present ... and Future?", *Int. J. Heat Fluid Flow*, Vol. 10, pp. 282-300.

Launder, B. E., and Shima, N., 1989, "Second Moment Closure for the Near Wall Sublayer: Development and Application", *AIAA Journal*, Vol. 27, pp. 1319-1325.

Lesieur, M., and Metais, O., 1996, "New Trends in Large-eddy Simulations of Turbulence", *Ann. Rev Journal of Fluid Mechanics*, Vol. 28, pp. 45-82.

Moser, R., Kim, D., and Mansour, N, 1999, "Direct Numerical Simulation of Turbulent Channel Flow up to $R_\tau = 590$", *Physics of Fluids*, Vol. 11, pp. 943-945.

Schiestel, R., 1987, "Multiple-time Scale Modeling of Turbulent Flows in one Point Closures", *Physics of Fluids*, Vol. 30, pp. 722-731.

Schiestel, R., and Dejoan, A., 2005, "Towards a New Partially Integrated Transport Model for Coarse Grid and Unsteady Turbulent Flow Simulations", *Theoretical and Computational Fluid Dynamics*, Vol. 18, pp. 443-468.

Speziale, C. G., Sarkar, S., and Gatski, T. B., 1991, "Modelling the Pressure-Strain Correlation of Turbulence: an Invariant Dynamical Systems Approach", *Journal of Fluid Mechanics*, Vol. 227, pp. 245-272.

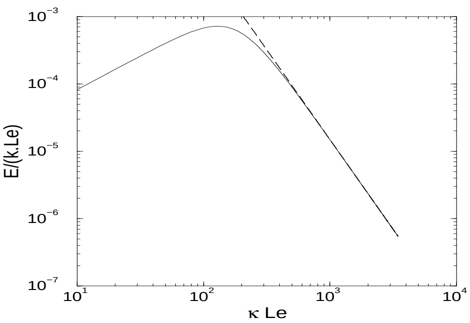

Figure 1: Analytical energy spectrum. - - -: $E(\kappa)/kLe = C_K(\kappa L_e)^{-5/3}$; —: $E(\kappa)/kL_e = \frac{2}{3}\beta(L_e\kappa)^2/\left[1+\beta(\kappa L_e)^3)\right]^{11/9}$

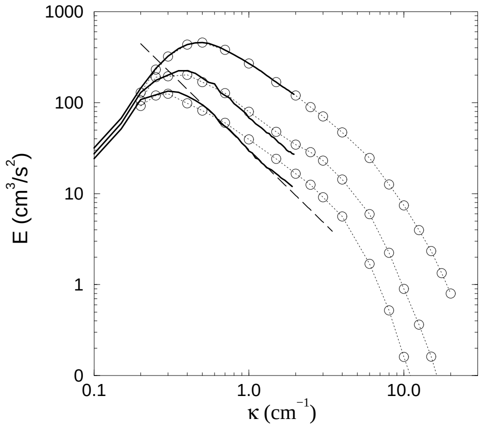

Figure 2: Homogeneous decay of the energy spectra ($\kappa_c = 2$ cm^{-1}). $\cdots\circ\cdots$: Comte-Bellot experiment ($t\,U0/M$ =42, 98 and 171); - - : Kolmogorov spectrum with $-5/3$ slope; —: PITM simulation.

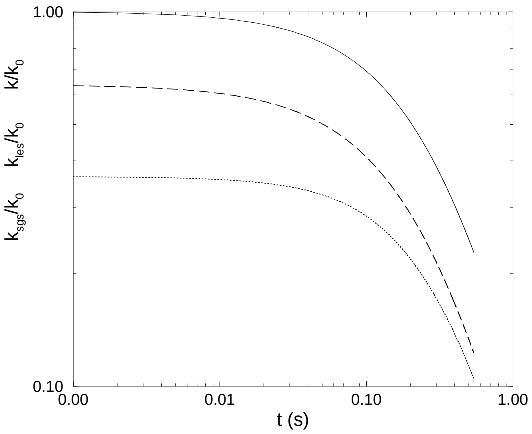

Figure 3: Homogeneous decay of the turbulent kinetic energy. ...: k_{sgs}/k_0 ; - -: k_{les}/k_0 ; —: $k/k_0 = (k_{sgs} + k_{les})/k_0$.

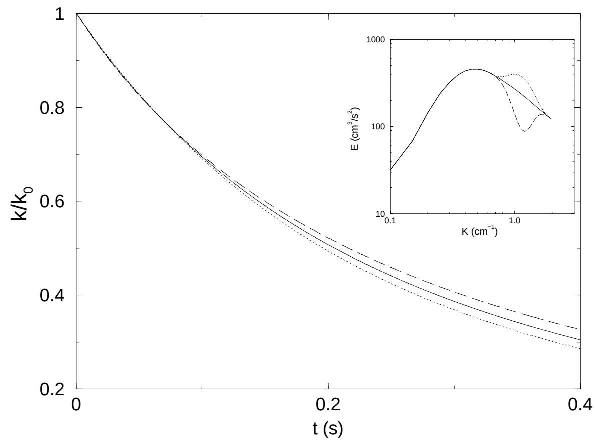

Figure 4: Homogeneous decay of the turbulent energy $k/k_0 = (k_{sgs} + k_{les})/k_0$; $\kappa_c = 2$ cm^{-1}; (α) : —; (β) ...; (γ) - - -.

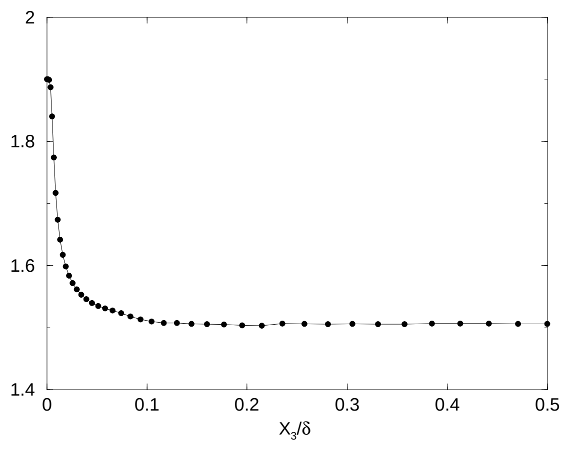

Figure 5: Subgrid-scale coefficient $c_{sgs\epsilon_2}$ obtained from relation (16).

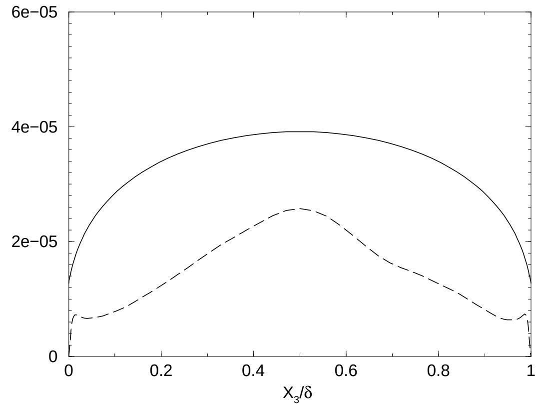

Figure 6: Subgrid length scale —: $\Delta = \pi/\kappa_c$; - - -: $L_{sgs} = \pi(3C_k/2)^{-3/2} k_{sgs}^{3/2}/\epsilon_{sgs}$

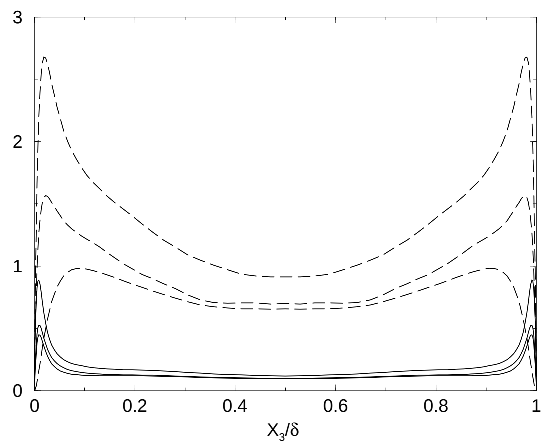

Figure 7: Subgrid and resolved normal stresses i=1,2,3 from top. SGS: —; LES: - - -.

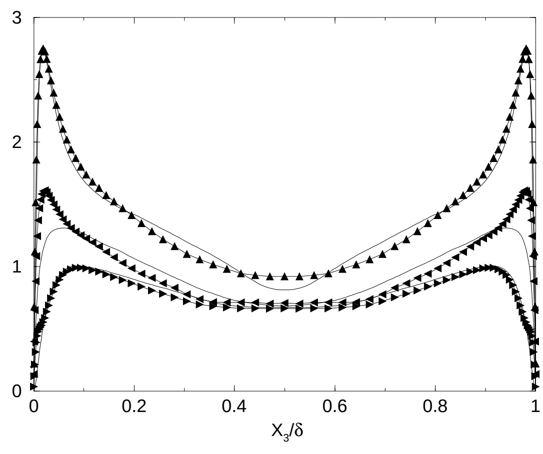

Figure 8: Total turbulent stresses $\left\langle (\tau_{ii})^{1/2} \right\rangle / u_\tau$. ▲ : $i = 1$, ◀: $i = 2$, ▶: $i = 3$. —: DNS.